crystals

MDPI

Article

Effect of Alginate from Chilean *Lessonia nigrescens* and MWCNTs on $CaCO_3$ Crystallization by Classical and Non-Classical Methods

Marianela Sánchez [1], Patricio Vásquez-Quitral [1], Nicole Butto [1], Felipe Díaz-Soler [1], Mehrdad Yazdani-Pedram [2], Juan Francisco Silva [3] and Andrónico Neira-Carrillo [1,*]

1 Department of Biological and Animal Sciences, Faculty of Veterinary and Animal Sciences, University of Chile, Santiago, P.O. Box 2-15, Chile; m.sanchez@ciq.uchile.cl (M.S.); pvasquitral@yahoo.com (P.V.-Q.); nbutto@veterinaria.uchile.cl (N.B.); fdiazsoler@gmail.com (F.D.-S.)
2 Faculty of Chemical and Pharmaceutical Sciences, University of Chile, Santiago, S. Livingstone 1007, Chile; myazdani@ciq.uchile.cl
3 Department of Material Chemistry, Electrocatalysis Laboratory, Faculty of Chemistry and Biology, University of Santiago de Chile, Santiago, P.O. Box 40-33, Chile; juan.silva.r@usach.cl
* Correspondence: aneira@uchile.cl; Tel.: +56-22-978-5642

Received: 23 December 2017; Accepted: 29 January 2018; Published: 31 January 2018

Abstract: In our crystallization experiments, the influence of alginate from Chilean *Lessonia nigrescens* and functionalized multi-walled carbon nanotubes (MWCNTs) was tested through electrocrystallization (EC) and gas diffusion (GD) methods on the crystal growth of calcium carbonate ($CaCO_3$) and their possible stabilization of proto-structures in amorphous $CaCO_3$ (ACC) state through pre-nucleation clusters (PNC) essays with automatic potentiometric titrations were performed. $CaCO_3$ crystals obtained in the in vitro above-mentioned crystallization systems were characterized by scanning electron microscope (SEM), energy-dispersive X-ray spectrometry (EDS) and powder X-ray diffractometer (XRD). Our experimental findings showed that ALG and functionalized MWCNTs stabilized truncated and agglomerated vaterite-like particles through GD and EC methods. While, on the other hand, we obtained qualitative information about induction or inhibition of $CaCO_3$ nucleation that was provided by potentiometric titrations.

Keywords: calcium carbonate; alginate; *Lessonia nigrescens*; electrocrystallization; multi-wall carbon nanotubes; potentiometric titration

1. Introduction

It is well known that living organisms produce advanced functional biogenic materials with precise control of morphology, size, polymorphism and crystal growth orientation. That control is governed by a diverse variety of biomolecules, including proteins and polysaccharides [1,2]. The effect of proteins and polysaccharides (PS) on biomineralization has been studied; however few studies have evaluated the mechanistic effect of PS on crystallization. For example, polycarboxylated PS regulate calcite growth and morphology in coccoliths [3,4]. Calcium carbonate ($CaCO_3$) is the most abundant inorganic biomineral in nature and has considerable industrial interest [5]. In order to achieve control over this biomineral, it is important to understand the mechanisms by which crystals are formed and the interaction between organic and inorganic components, as it occurs in nature. In the last decade, the role of inorganic precursor species (IPS), such as amorphous phases and pre-nucleation clusters (PNCs) has become relevant [6]. PNCs of $CaCO_3$ occur before the formation of metastable solid nucleus of amorphous $CaCO_3$ (ACC) and this was initially seen with measurements with a calcium ion-selective electrode and pH-titration during the early stages of precipitation (pre- and post-nucleation) [7]. The

existence of PNCs in homogeneous solutions has been evidenced for the most important biominerals, calcium phosphates and carbonates, iron oxides, silica and organic compounds such as amino acids [8]. Thus, potentiometric titration has become an excellent technique to study the influence of additives in the overall process of precipitation [9]. $CaCO_3$ has more than one amorphous phase (polyamorphism) identified as proto-calcite (pc-ACC), proto-aragonite (pa-ACC) and proto-vaterite (pv-ACC) by the local arrangement of atoms [10,11].

In an attempt to understand the effect of PS on the early stages of crystallization, short chain sugars have been tested by using automatic potentiometric titrations [12]. In this regard, it is demonstrated that the nature of glycosidic linkages, polarity, ion binding sites and stereochemistry has strong influence on $CaCO_3$ crystallization [13]. With this in mind and following our previous results, here we used an alginate (ALG) sample obtained from Chilean brown algae *Lessonia nigrescens* (ALG *Les*) in order to add more experimental evidence to the relationship between PS and IPS [12,14–16]. In this work, we investigated the direct effect of ALG *Les*, extracted from a natural brown algae located in north of Chile, on early stages of $CaCO_3$ mineralization. ALG is a linear copolymer composed of two monomeric units: β-D-mannuronic acid (M) and α-L-guluronic acid (G), where the M and G units are $1 \rightarrow 4$ linked by glycosidic bonds. The M and G homopolymeric blocks are distributed along the copolymeric chain and region of MG blocks. The ratio and location of M and G units are critical factors for their physicochemical properties such as affinity to cations, gelification and hydrogel behaviors and chain rigidity. ALGs are relevant to crystallization because G units can interact with divalent cations through binding sites [17]. On the other hand, it is known that organic hydrogels play an important role in $CaCO_3$ biomineralization in corals and mollusks [18]. Therefore, the investigation of the influence of PS hydrogels such as ALG on $CaCO_3$ crystallization through classical and non-classical methods is necessary. Rounded calcite crystals have been obtained through gas diffusion (GD) method by using ALG [19]. ALG does not alter the typical rhombohedral calcite form on $CaCO_3$ crystallization [20] and it has shown inhibiting capacity by adsorption onto the active growth sites of the crystal surface [21]. Also, "rosette-like" $CaCO_3$ aggregates have been obtained by direct mixing of Ca^{2+} and CO_3^{2-} ions in the presence of sodium ALG [22]. Ma and Feng used Ca-ALG beads as a slow and continuous source of Ca^{2+} ions into Na_2CO_3 solution. Crystal size, morphology and surface roughness were influenced by the type of ALG used in the crystallization experiments, which could be accounted by the length of the G blocks [22]. Our group extracted and purified ALG from Chilean algae. The purified ALG was used for microencapsulation of parathyroid gland cells from human patients showing good viability and sustained release of PTH hormones [23]. To our knowledge, most of the investigations have addressed the effect of ALG on $CaCO_3$ mineralization in terms of morphology and polymorphism of the resulting crystals by using only GD as a classical method. In general, the structure and stability of IPS and chemical nature of the additives influence the characteristics of inorganic minerals, including the formation of superstructures, inhibition of the nucleation, and stabilization of different polymorphs, among others [24].

Additionally, carbon-based materials have been investigated as nanomaterials-controlled crystallization [25]. Carbon nanotubes (CNTs) have become an attractive material due to: large energy absorbing capacity, electrical conductivity, chemical stability, low density, high aspect ratio, stiffness, etc. [26]. CNTs have been proved an efficient heterogeneous nucleating agents that can accelerate the crystallization of several inorganic materials, including cement, silicon nitride and zirconium oxide [27–29]. The effect of pristine and functionalized single-walled CNT (SWCNT) and multi-walled CNT (MWCNT) on $CaCO_3$ mineralization has been also investigated. Typical calcite and spherical or ellipsoidal $CaCO_3$ crystals were obtained when pristine CNTs and modified CNTs were utilized as templates [30]. In other work, CNT favored the formation and stabilization of vaterite crystals [31]. Therefore, it is very important to introduce alternative classical methods such as electrocrystallization (EC) for in vitro $CaCO_3$ mineralization. For instance, very few studies have reported the effect of commercial ALGs on crystal growth of $CaCO_3$ by using an electrochemical approach [32]. In addition,

for a better understanding of the events of PNCs on $CaCO_3$ mineralization in the presence of ALG as natural PS and carbon nanomaterials, quantitative techniques are necessary.

Herein, we evaluated the effect of ALG *Les* from *Lessonia nigrescens*, and pristine MWCNT and functionalized MWCNT and their combination, on the different stages of $CaCO_3$ crystallization using EC and GD techniques and automatic potentiometric titrations as classical and non-classical crystallizations, respectively.

2. Materials and Methods

2.1. Reactants

Calcium chloride dihydrate ($CaCl_2 \cdot 2H_2O$), sodium bicarbonate ($NaHCO_3$), sodium hydroxide (NaOH), sodium chloride (NaCl) and potassium nitrate (KNO_3) were obtained from Merck. Sodium alginate extracted from *Lessonia nigrescens* (ALG *Les*) was purified in ethanol by using soxhlet purification protocol [23]. MWCNTs were purchased from Bayer (Bayer, Germany). According to the manufacturer's specifications, the average diameter and length of MWCNTs were 30 nm and tens micrometer, respectively, with 95% purity. Indium tin oxide (ITO) conductive glass electrodes used as conductive material on EC of $CaCO_3$ were purchased from Delta Technologies (Dallas, TX, USA). In case of MWCNT-COOH and MWCNT-OX materials were gently provided by the laboratory of electrocatalysis of the University of Santiago de Chile (Dr. J.F. Silva) and laboratory of polymer chemistry of the University of Chile (Dr. M. Yazdani-Pedram), respectively.

2.2. In Vitro Gas Diffusion (GD) Crystallization of $CaCO_3$.

GD crystallization of $CaCO_3$ crystals in the presence of ALG *Les* and MWCNTs derivatives as polymeric additives was carried out at room temperature for 24 h. GD method was performed as we described in our previous works [33–36].

2.3. Electrodeposition of Alginate/MWCNTs.

For the preparation of ALG-MWCNTs/ITO electrodes, $CaCO_3$ powder (0.25%) was blended into ALG *Les* solution (12.5 g/L), and sonicated during 30 min. After, 1.6 mg of MWCNTs were added to the above solution (ALG/MWCNT/$CaCO_3$), and this new mixture was ultrasonicated for 5 min at room temperature in order to obtain a black and homogeneous suspension, containing 0.08 mg mL^{-1} MWCNTs. Then, an ITO coated glass slide was partially immersed (1.25 cm × 1.0 cm) into this deposition solution, and an anodic voltage was applied to achieve a current density of 3 $A \cdot m^{-2}$ during 2 min. After electrodeposition, ITOs electrodes were removed from the solution, rinsed with nanopure water and air dried prior to electrochemical measurements [37].

2.4. Electrocrystallization (EC) Experiments of $CaCO_3$.

EC essays were performed onto ITO glass surface into the glass electrochemical cell using a galvanostat/potentiostat BASi Epsilon (USA) instrument. Chronoamperometry was used during the $CaCO_3$ electrocrystallization. ITO working electrodes from Corning® aluminosilicate glass, 25 × 25 × 1.1 mm, coated with one surface of RS = 5–15 Ω was used. ITO were washed with methanol and Milli Q water, obtained from a water purification system LaboStar 4-DI/UV and sonicated them during 5 min. The electrochemical measurements were conducted in pieces of ITO as working electrodes (WE), a coiled platinum (Pt) wire was used as auxiliary electrode (AE) and a silver chloride electrode (Ag/AgCl) as reference electrode (RE). For the electrochemical reaction we used an electrolyte solution with dissolved O_2, at a basic pH and at room temperature. The electrolytic solution consisted of 0.2 mM $CaCl_2$, 6 mM $NaHCO_3$ and 10 mM NaCl. For the EC of $CaCO_3$, a linear sweep voltammetry was also performed in order to determine first the potential maximal value where O_2 reduction reaches the maximum voltage activity, that is, −890 mV. This potential value was fixed and further used for the chronoamperometry technique performed on $CaCO_3$ coating for 120 min [32,38].

2.5. Prenucleation Clusters (PNC) Assay of $CaCO_3$

PNC essays were conducted by direct automatic potentiometric titrations using a titration system (Titrando 907) from Metrohm (Herisau, Switzerland), with two dosing units (Dosino 800), controlled by software (Tiamo v2.2). 10 mM $CaCl_2$ was added at a rate of 0.01 mL/min into 20 mL sample solution in a 50 mL beaker while stirring at 900 r.p.m. Then, pH was kept constant at 9.00 by automatic counter-titration of 0.01 M NaOH. The pH and free Ca^{2+} concentration in the samples were monitored by a glass electrode (Metrohm, No. 6.0256.100) and a Ca^{2+} ion-selective electrode (ISE, Metrohm, No. 6.0508.110), respectively. Between experiments, beaker and electrodes were cleaned with acetic acid to remove precipitated $CaCO_3$ particles, followed by multiple rinsing with water. The Ca^{2+}-ISE was calibrated regularly by titrating $CaCl_2$ into 20 mL water (adjusted to pH 9.00 by addition of NaOH) using the above-mentioned procedure. All titrations were performed at room temperature with a minimum of three repetitions [6,12,13].

2.6. Characterization

The surface morphology of the resultant $CaCO_3$ crystals was characterized by scanning electron microscopy (SEM) using a JEOL JSM-6390LV (Tokyo, Japan) and HITACHI TM3000 (Hong Kong, China) instruments. The XRD diffraction spectra were taken from a powdered $CaCO_3$ sample using a Siemens D-5000 X-ray diffractometer (Siemens, Munich, Germany).

3. Results and Discussion

EC and GD classical methods were utilized in order to evaluate the morphogenetic effect of Chilean ALG *Les*, pristine MWCNT and oxidized MWCNT (MWCNT-OX) on $CaCO_3$ crystal growth. In addition, non-classical PNCs essays through automatic potentiometric titrations showed a possible mechanism of early action of these additive compounds. GD crystallization was carried out for 24 h at room temperature. Figure 1 shows SEM images of $CaCO_3$ crystals grown without additive as control (Figure 1A), and in the presence of additives at 2 mg/mL ALG *Les* (Figure 1B), 1 mg/mL MWCNT (Figure 1C), 1 mg/mL MWCNT-OX (Figure 1D), mixtures of ALG *Les*/MWCNT (Figure 1E) and ALG *Les*/MWCNT-OX (Figure 1F). Figure 1A shows typical rhombohedral calcite crystals of size 20–50 µm, while Figure 1B shows individual and aggregated calcite crystals in the presence of ALG *Les* as additive. These experimental results are in agreement with the non-modified calcite form already reported by several authors who used commercial ALGs [39]. However, when spin coated ALG was used as oriented support for $CaCO_3$ GD method, abundant calcite and vaterite particles were obtained [40]. Figure 1C shows that when MWCNT was used as additive for $CaCO_3$ mineralization, mainly single calcite crystals were formed. We found that at increasing concentration of MWCNTs, higher quantity of small calcite crystals appeared (see Supplementary Material, Figure S1). In consequence, MWCNT induced large quantity of small calcite crystals in comparison to control experiment. Furthermore, experimental set up under agitation causes the production of smaller crystals (see, Figure S2). These indicate that MWCNT may act as nucleation sites in the above-described assays, favoring larger amount of $CaCO_3$ crystals. On the other hand, numerous calcite crystals and agglomerated vaterite-like particles were stabilized in the presence of MWCNT-OX (Figure 1D). Resultant $CaCO_3$ crystals of 30–50 µm were formed with ALG *Les* combined with MWCNT or MWCNT-OX. The overall results with MWCNTs are in agreement with Tasis et al. who utilized GD method for $CaCO_3$ mineralization with non-modified MWCNT and non-covalently modified MWCNT with amphiphilic isoprene-*b*-acrylate copolymer [30]. $CaCO_3$ crystals grown on non-modified MWCNT substrate showed similar rhombohedral calcites, while modified MWCNT substrate induced ellipsoidal or spherical crystals. These morphological changes can be attributed to the interactions between the carboxylic and hydroxyl groups and specific faces of the growing $CaCO_3$ crystals. Moreover, Li et al. proved the influence of carboxylated SWCNT and MWCNT on spherical vaterite stabilization [31]. Herein, we evaluated the effect of the combination of ALG *Les*/MWCNT and ALG *Les*/MWCNT-OX

as additive on $CaCO_3$ crystallization. Our findings showed a synergic effect when ALG *Les*/MWCNT mixture was used, indicating an effective stabilization capacity. In this case, isolated calcite crystals of 10–30 μm with well-defined edges were observed (Figure 1E). Moreover, when ALG *Les*/MWCNT-OX mixture was used, small truncated calcites of 5–10 μm with rounded edges were obtained due to the active surface of combined additives. These rounded edges can be due to the deposition of a thin organic layer underneath, evidenced by the bright background, causing differences in conductivity and brightness of the image (Figure 1F).

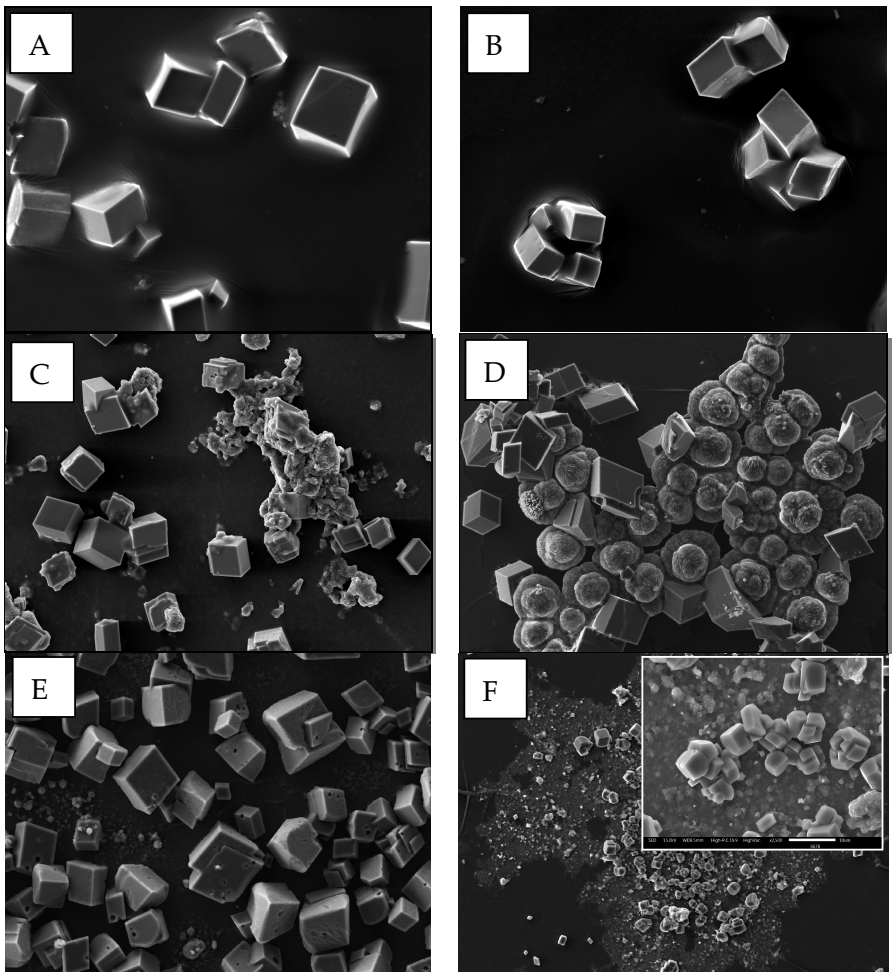

Figure 1. SEM images of $CaCO_3$ crystals obtained by using GD crystallization. Control (**A**), ALG *Les* (**B**) MWCNT (**C**), MWCNT-OX (**D**), ALG *Les*/MWCNT (**E**) and ALG *Les*/MWCNT-OX (**F**). Scale bar = 50 μm. Inset scale bar = 10 μm.

In order to determine the internal lattice of crystalline $CaCO_3$ products, X-ray diffraction (XRD) technique was performed. Figure 2 shows XRD pattern of $CaCO_3$ crystals obtained by GD method without an additive as control (Figure 2A), and in the presence of ALG *Les* (Figure 2B), MWCNT (Figure 2C), MWCNT-OX (Figure 2D), mixtures of ALG *Les*/MWCNT (Figure 2E), and ALG *Les*/MWCNT-OX (Figure 2F). In general the XRD spectra shows crystalline peaks with slight difference in the intensity of the main reflections from calcite (104) and vaterite (101), suggesting that the obtained inorganic product mainly consisted of mixed phases of calcite and vaterite particles. Although the integrate intensity of the (104) reflections from calcite at ca. $2\theta = 30^\circ$ and vaterite at ca. $2\theta = 25^\circ$ were not used to determine the relative amount of the calcite and vaterite, the calcite polymorphism in the resultant inorganic deposition was higher as observed by SEM analysis. It is interesting to note that the XRD analysis clearly showed a new diffraction peaks at $2\theta = 56.7^\circ$, which is ascribed to (202)

crystallographic face of vaterite when ALG *Les* (Figure 2B) and MWCNT-OX (Figure 2D) and their respective mixtures of ALG *Les*/MWCNT (Figure 2E) and ALG *Les*/MWCNT-OX (Figure 2F) were used as additives.

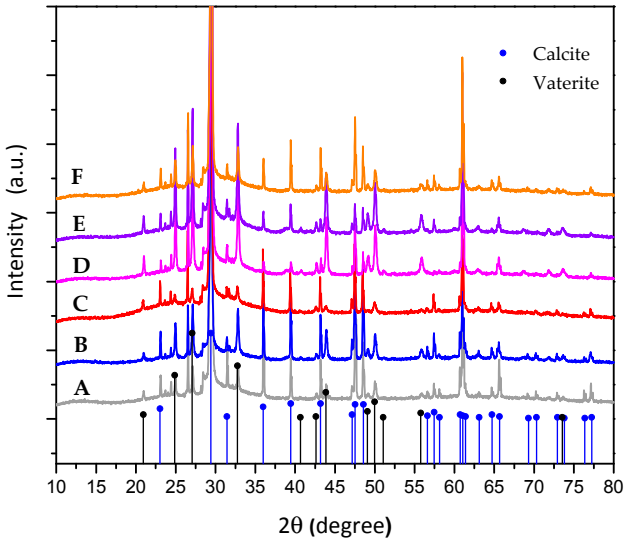

Figure 2. XRD pattern of $CaCO_3$ crystals obtained by GD crystallization: Control (**A**), ALG *Les* (**B**), MWCNT (**C**), MWCNT-OX (**D**), ALG *Les*/MWCNT (**E**) and ALG *Les*/MWCNT OX (**F**). Vertical blue line and black line designation in graph indicate calcite and vaterite standard peaks, respectively.

We believe that different complementary crystallization methods can be used to address the effect of ALG *Les* and MWCNT on the in vitro $CaCO_3$ mineralization. With this in mind, a second in vitro crystallization method by an electrochemical approach was carried out. The EC method corresponds to a heterogeneous system, in which abundant and uniform $CaCO_3$ crystals on ITO electrode were formed. The general scheme of EC of $CaCO_3$ onto ITO substrate is illustrated in the supplementary material (see Figure S3). The electrolyte solution composed of $Ca(NO_3)_2$, $NaHCO_3$ and NaCl with dissolved molecular oxygen (O_2) was used at alkaline pH solution media and the electrochemical reduction of O_2 is promoted by applying a sufficiently negative potential. The electro-reduction produces a local increment of pH, which in turn induces the bicarbonate (HCO_3^-) ions present at the interface to become carbonate (CO_3^{-2}), thus the precipitation of $CaCO_3$ is achieved [32]. Deposited $CaCO_3$ crystals onto ITO surface are not conductive, reducing the active area of the ITO electrode. Consequently, the total cathodic current decreases, which can be measured by chronoamperometry [41]. Therefore, a set of ITO substrates with ALG and MWCNTs separately and mixed through EC of $CaCO_3$ by electrodeposition was carried out. The resultant crystals were then analyzed by scanning electron microscopy SEM (Figure 3) and chronoamperometry. The chronoamperometric curves of EC of $CaCO_3$ in the absence of additive (control; Figure S4A) and in the presence of ALG *Les* (Figure S4B) can be seen in the Supplementary Material, Figure S4. SEM analysis showed that when EC essays were performed on bare ITO (Figure 3A) rhombohedral calcite and circular vaterite were formed in a similar proportion. When the EC was performed on ALG *Les* on modified ITO, isolated rhombohedral calcite and spherical $CaCO_3$ superstructures composed of small and aggregated calcite were observed (Figure 3B). Similar "rosette-like" calcite was obtained in the presence of pectin as additive on $CaCO_3$ crystallization [42]. Moreover, when EC of $CaCO_3$ was performed on modified ALG *Les*/MWCNT-ITO, a great quantity of agglomerated small calcite and spherical metastable vaterite particles were produced (Figure 3C). Surprisingly, in the presence of ALG *Les*/MWCNT-OX mixture on modified ITO, agglomerated vaterite and calcite crystals were stabilized (Figure 3D). In this case, the presence of chemical moieties e.g., hydroxyl group in MWCNT-OX could influence the $CaCO_3$ mineralization explaining the huge amount and size of the metastable form of vaterite particles.

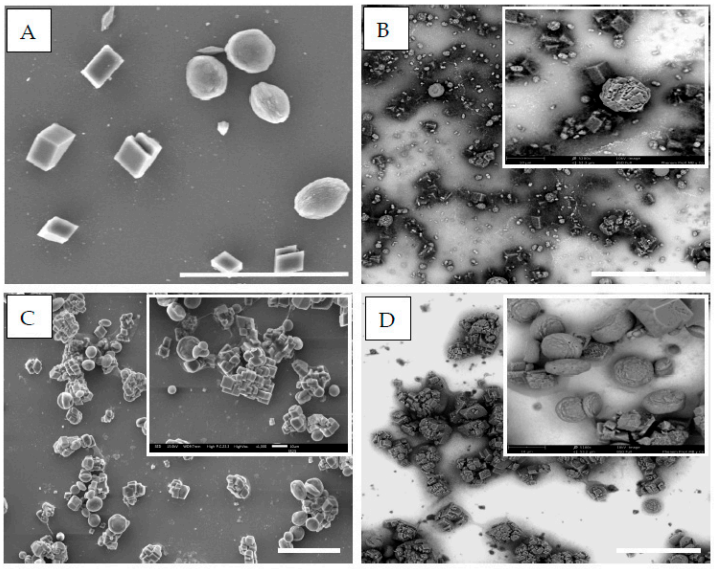

Figure 3. SEM images of $CaCO_3$ crystals obtained through EC on modified ITO electrodes: control (bare ITO) (**A**), ALG *Les* modified ITO (**B**), ALG *Les*/MWCNT modified ITO (**C**), ALG *Les*/MWCNT-OX modified ITO (**D**). Scale bar = 50 μm. Inset scale bar = 10 μm.

Moreover, grazing incidence X-ray diffraction (XRD) measurements of the bare ITO glass substrate and $CaCO_3$ particles obtained on modified ITOs through EC is shown in Figure 4. Grazing incidence XRD analysis was performed on ITO electrode because of strong ITO interference and low quantity deposited inorganic mineral. The principal crystalline peaks of bare ITO substrate (green line) at 2θ = 31.7° (Figure 4A), and $CaCO_3$ particles on bare ITO (black line) (Figure 4B) and in the presence of MWCNT-OX and ALG *Les* at 2θ = 30° suggested that the calcite polymorph was the principal product. Although all crystalline peaks ascribed to the diffraction of calcite, less thermodynamically vaterite polymorphs was also observed (Figure 4D). A broad peak in the range of 2θ = 8–18° was observed only when ALG *Les*, ALG *Les*/MWCNT or ALG *Les*/MWCNT-OX were used as additive. This fact is due to semi-crystalline nature of sodium ALG, showing peaks at 2θ = 12.81°, 21.83°, 23.25°, 35.9° and 39.92° [43,44].

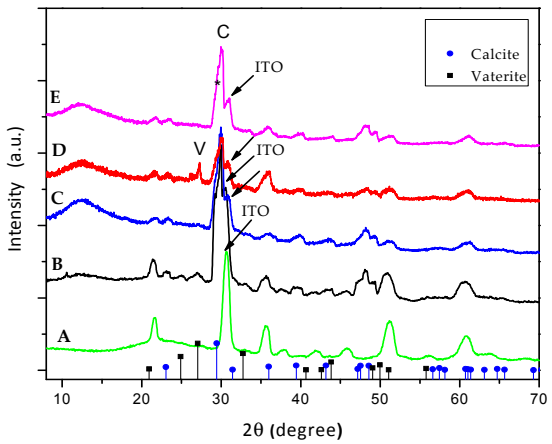

Figure 4. XRD pattern of ITO substrate (**A**) and $CaCO_3$ crystals obtained through EC in the presence on bare ITO as control (**B**), ALG *Les* modified ITO (**C**), ALG *Les*/MWCNT modified ITO (**D**), ALG *Les*/MWCNT-OX modified ITO (**E**), Vertical blue line and black line designation in graph indicate calcite and vaterite standard peaks, respectively. Meanwhile, designation C, V and * correspond to (104) face of calcite and ITO signal, respectively.

To gain a better understanding of the effect of ALG *Les* and MWCNTs on in vitro $CaCO_3$ obtained through GD and EC methods, a non-classical technique was conducted by direct automatic potentiometric titrations using PNCs essays at pH 9.0. The advantage of PNCs methods lies in the fact that is possible to obtain information regarding the changes of slope before nucleation, nucleation time and solubility product after nucleation, among others directly from the $CaCO_3$ crystallization kinetic curves. Therefore, induction or inhibition effect of additives on pre-nucleation of $CaCO_3$ species and the additives according to their effect on titration essays can be classified as follows. Type I, complexation of Ca^{2+} ions (delayed initial increase in free Ca^{2+}), type II, influence on the PNC equilibriums in solution (change in the slope of the curve before nucleation), type III, effect on nucleation, inhibition (IIIa) or promotion (IIb) of nucleation, type IV, adsorption onto nucleated particles, and type V, modification of the structure and stability of the initially precipitated phase, giving liquid-like, amorphous or crystalline polymorphs (after nucleation) [13,24].

With this in mind, we studied the control assay of $CaCO_3$ nucleation time, that was 6.300 s and the ion product measured as 3.21×10^{-8} M^2 after nucleation (Figure 5), which is slightly higher but in concordance with the solubility values reported for the proto-calcite (ACC I or pc-ACC) formed at pH 9.0 [6]. When the titration experiments were performed in the presence of ALG *Les* at two concentrations, a direct relationship between nucleation time and the concentration of ALG *Les* was found (Figure 5). There was a slight decrease in the pre-nucleation slope observed with ALG *Les* at 5 mg/L, indicating an increase in the complexed Ca^{2+} ions during mineralization. These results suggest the stabilization of amorphous PNC species. Moreover, the solubility product observed was close to the value obtained for the control assay. However, when ALG *Les* at 10 mg/L was utilized, the value of the solubility product reaches that of ACC species representing the more soluble initial stages of unstable amorphous entities (Figure 5). These results are in agreement with the previous $CaCO_3$ mineralization by classical methods using ALG *Les*, where proto-structures are stabilized. This behavior has been previously documented, where ALG favors the formation of ACC state. Leng et al. proposed a mechanism for the formation of saucer-like structures in which Ca^{2+}-ALG interactions stabilizes aggregated proto-structures of ACC particles [45]. According to our PNC essays, lower concentration of ALG *Les* selectively controls the in vitro $CaCO_3$ mineralization by direct interaction of ACC surfaces through PNC essays. The possible mechanisms of ALG *Les* on $CaCO_3$ nucleation could be explained by PNC equilibriums in solution (type II), inhibition of nucleation (type IIIa) and by the solubility product changes (type V).

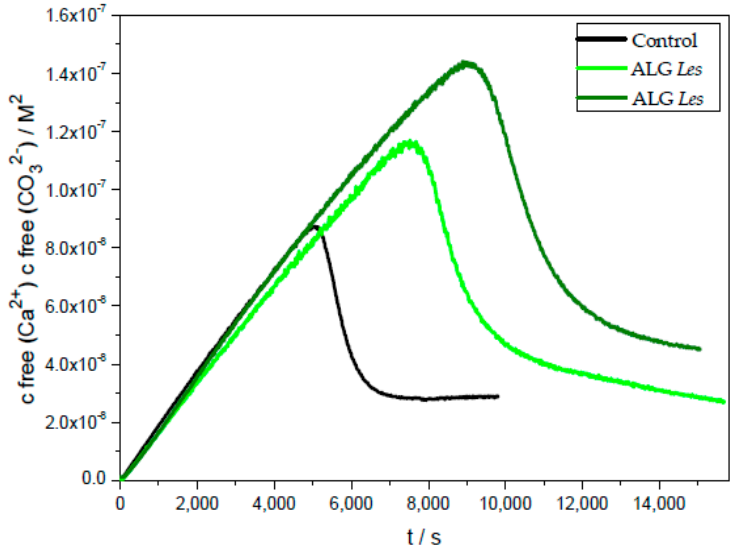

Figure 5. Time development of $CaCO_3$ solubility products using two concentrations of ALG *Les* at pH 9.0: blank (**black line**), 5 mg/L ALG *Les* (**green line**) and 10 mg/L ALG *Les* (**olive line**).

Moreover, evolution of the solubility product was studied in the presence of MWCNT at 2.5 and 7.5 mg/L concentrations as is shown in Figure 6. Both concentrations were selected since previous studies indicated an observable effect on the $CaCO_3$ crystallization by this method [46]. As seen in Figure 6 no difference in the slopes of the curves and solubility products was noticed, however a notorious decrease of nucleation time was observed. Specifically, nucleation time decreased to 5.000 s for both concentrations in comparison to the control essay registered at 6.250 s. Therefore, this additive at this concentration acted as strong promoter of $CaCO_3$ crystallization. We also found that the concentration MWCNT does not affect the nucleation time. This is a characteristic of heterogeneous nucleation, where $CaCO_3$ crystals are in contact with MWCNT. No chemical interaction between $CaCO_3$ and pristine MWCNT exists due to the absence of polar functional groups on the surface of MWCNT, thus the final solubility product value remains unaltered. These results can be related to preliminary empirical observations, in which pristine MWCNTs induced the formation of small $CaCO_3$ particles that may randomly contact each other, therefore the crystals can grow on MWCNTs [31]. Other studies have shown similar nucleating activity as this current study. Some examples included nucleation and growth of hydroxyapatite crystals on functionalized SWCNT [47]. They found that SWCNT accelerate the rate of the hydration reaction of tricalcium silicate in the ordinary Portland cement acting as a nucleating site [27]. According to our PNC essays, the influence of pristine MWCNT on the $CaCO_3$ mineralization showed an induction capacity on the nucleation time (type IIIb), however this did not affected the pre-nucleation slope and the solubility product of nucleated phase.

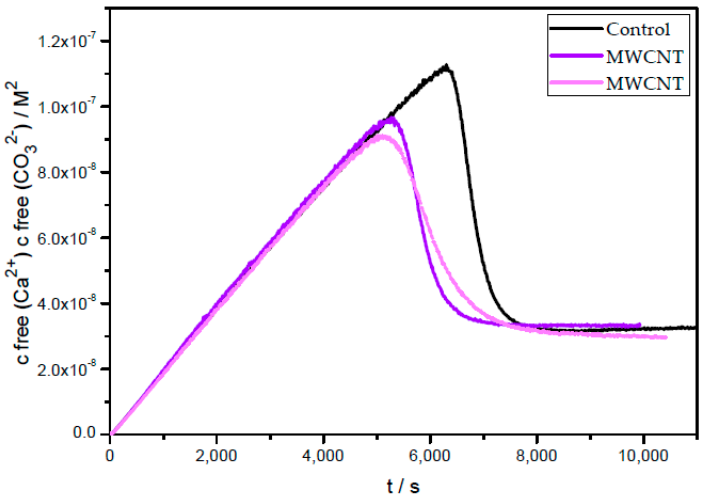

Figure 6. Time development of $CaCO_3$ solubility products using two concentration of MWCNT at pH 9.0: blank (**black line**), 2.5 mg/L MWCNT (**purple line**) and 7.5 mg/L MWCNT (**magenta line**).

In order to evaluate the effect of functionalized MWCNT-COOH on the PNCs experiments, MWCNT containing predominantly carboxylic groups was used as additive at 2.5 mg/L (Figure 7). Our findings showed a notorious decrease in the slope of the free Ca^{2+} curve before nucleation, indicating a strong interaction of the MWCNT-COOH with Ca^{2+} ions and suggesting the PNCs stabilization. The nucleation time is ca. 2.5 times greater than the control experiment, indicating that functionalized MWCNT act as an effective inhibitor of the nucleation of $CaCO_3$ and stabilizing the proto-structure of ACC entities. Accordingly, the influence of MWCNT-COOH on the $CaCO_3$ mineralization obeys the following mechanism: PNC equilibriums in solution (type II) and inhibits nucleation (type IIIa). These findings are in agreement with previous studies, which showed that MWCNT-OX can alter the nucleation, growth and aggregation of $CaCO_3$ crystals under classical crystallization conditions.

With the above-mentioned results obtained with ALG *Les* at lowest concentration (5 mg/L), the evolution of the solubility product was studied in mixture with two concentrations of MWCNT at

2.5 mg/L (Figure 8A) and at 7.5 mg/L (Figure 8B). Figure 8A (orange line) shows a similar decrease in the slope of the free Ca^{2+} curve before nucleation, indicating interaction of the additive surface with Ca^{2+} ions and inhibition of the nucleation similarly to ALG *Les*. Moreover, the solubility product observed here was close to the value obtained for the control assay. However, when the evolution of the solubility product was evaluated in mixture but with the higher concentration of MWCNT (7.5 mg/L), the slope of the free Ca^{2+} curve before nucleation was similar to ALG *Les*, but the presence of MWCNT 7.5 mg/L affected the overall results (Figure 8B). In this manner, a decrease of the nucleation time was observed, showing a less powerful inhibition of the nucleation time than with ALG *Les* as additive. At the end, the solubility product obtained with this mixture had a lower value than the control assay indicating stabilization of ACC proto-structures.

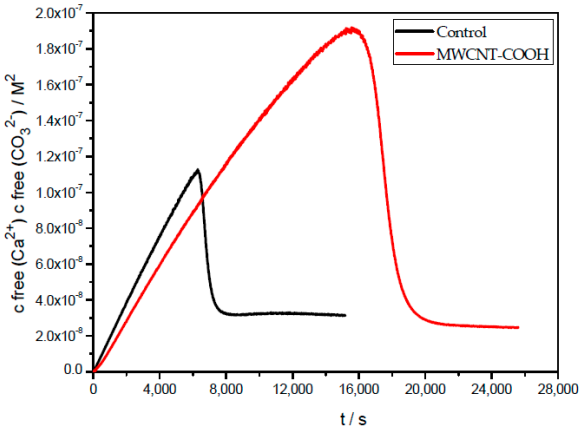

Figure 7. Time development of $CaCO_3$ solubility products using 2.5 mg/L MWCNT-COOH at pH 9.0: control (**black line**) and 2.5 mg/L (**red line**).

Figure 9 shows the evolution of the solubility product using the ALG *Les* with functionalized MWCNT-COOH. Our experimental curves showed a decrease in the slope of the free Ca^{2+} curve before nucleation indicating the strongest interaction of additive surface with Ca^{2+} ions, and inhibition of the nucleation here was similar to MWCNT-COOH and the solubility product value is higher than those of control and MWCNT-COOH. These results indicate that the optimum additive for inhibiting the nucleation of $CaCO_3$ is the mixture of ALG *Les* with MWCNT-COOH, in which the evolution of the solubility product shows almost the same effect of MWCNT-COOH alone. It is concluded the best synergetic effect is achieved when a strong interaction exists between components of additives with inhibiting activity.

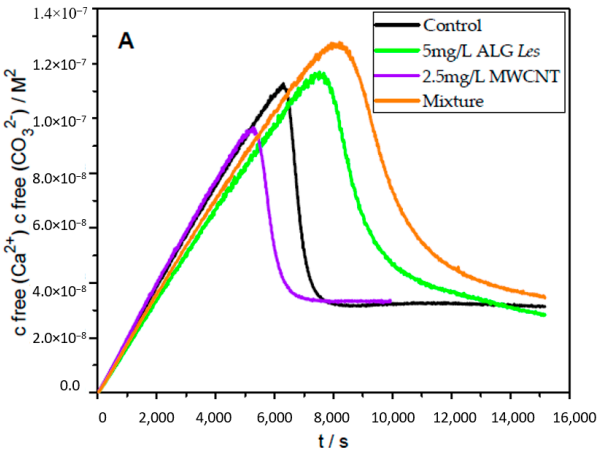

Figure 8. *Cont.*

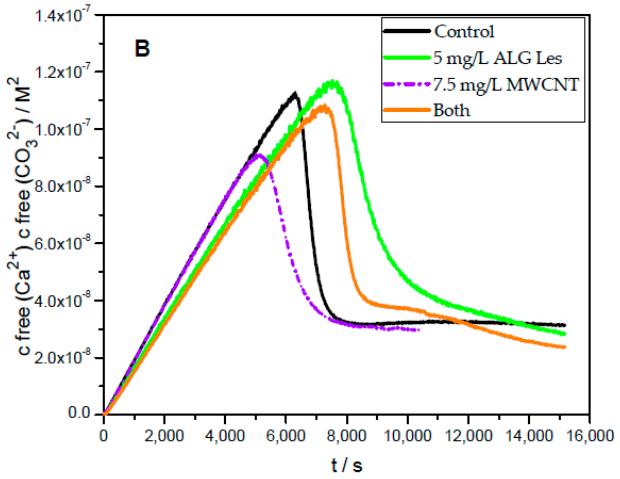

Figure 8. Time development of $CaCO_3$ solubility products using 5 mg/L ALG *Les* and MWCNT of 2.5 mg/L (**A**) and 7.5 mg/L (**B**) concentrations at pH 9.0: Blank (black line), 5 mg/L ALG *Les* (green line), 2.5 mg/L MWCNT (purple straight line) and 7.5 mg/L MWCNT (purple dash dot line), and both in mixture (orange line).

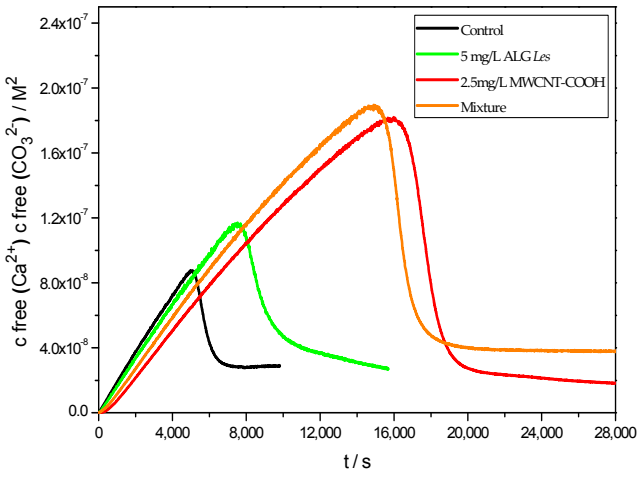

Figure 9. Time development of $CaCO_3$ solubility products using ALG Les and MWCNT-OH at pH 9.0: blank (**black line**), 5 mg/L ALG *Les* (**green line**), 2.5 mg/L MWCNT-COOH (**red line**), and both in mixture (**orange line**).

4. Conclusions

We demonstrated that by using classical methods such as GD and EC, a synergic effect of the mixture of ALG *Les* and MWCNT on the in vitro $CaCO_3$ mineralization was obtained indicating an effective stabilization. Moreover, the XRD analysis showed the main reflections from calcite and the less thermodynamically stable polymorph vaterite particles as the main inorganic products. On the other hand, non-classical methods through automatic potentiometric titrations essays clearly demonstrated the direct relationship between nucleation time and the concentration of additives. The pre-nucleation slope indicated complexed Ca^{2+} ions with additive surface during mineralization, stabilization of amorphous proto-structure of ACC, etc. showing a quantitative data of the entire crystallization process of additives at pre-and post-nucleation state. Therefore, by using simultaneously both crystallization approaches, we can further understand how biomacromolecules act as inductor or inhibitor and selectively control the crystal growth, size and polymorphism of biogenic mineral in a similar manner that occurs in nature.

Supplementary Materials: The following are available online at http://www.mdpi.com/2073-4352/8/2/69/s1. Figure S1: SEM images of $CaCO_3$ obtained through GD showing the effect of MWCNT concentration on number and size of calcite particles. Figure S2: Effect of agitation on the resultant $CaCO_3$ crystals. Figure S3: Scheme of EC of $CaCO_3$ onto ITO. Figure S4: Chronoamperometric curves of EC of $CaCO_3$ in absence of additive (control) and additives such as pristine MWCNT, ALG Les, MWCNT-OX and mixed of ALG *Les*/MWCNT and ALG *Les*/MWCNT-OX.

Acknowledgments: This research was supported by FONDECYT 1171520, ACCDiS 15130011 granted by the Chilean Council for Science and technology (CONICYT), and funded by the Program U-Redes, Vice-presidency of Research and Development, University of Chile. Marianela Sánchez thanks CONICYT scholarship 21120326.

Author Contributions: Marianela Sánchez, Patricio Vásquez-Quitral, Nicole Butto, Felipe Díaz-Soler conceived, designed and performed the experiments; Marianela Sánchez and Andrónico Neira-Carrillo wrote the paper. Mehrdad Yazdani-Pedram and Juan Francisco Silva contributed with manuscript supervision. Andrónico Neira-Carrillo contributes with reagents/materials/analysis tools and represents the senior author, and he is principal investigator of the 1171520 FONDECYT project and Program U-Redes, Vice-presidency of Research and Development, University of Chile, in which the current research work were realized. Therefore, Andrónico Neira-Carrillo gives the first author the intellectual input, designs and approves the reported protocols of this study. Andrónico Neira-Carrillo and Mehrdad Yazdani-Pedram have been responsible for the manuscript correction, proof reading during all paper submission, handling the revisions and re-submission process of the revised manuscript.

Conflicts of Interest: The authors declare no conflict of interest.

Appendix

Appendix A.1 ALG Extraction from L. nigrescens

ALG extraction from algae was conducted using a modified extraction method described in literature [48]. Resultant ALG sample of various ALG particle sizes were obtained from dried *L. nigrescens* by mechanical crushing and screening were obtained. Briefly, 10 g of algae were ground on a Thomas-Wiley laboratory mill, model 4, wetted with 400 mL of distilled water under vigorous stirring and acidified with HCl 0.1 M solution to pH 4. This mixture was stirred for 15 min at room temperature and then the supernatant was removed. This pre-treatment was repeated three times on each sample, each time using 40, 25 and 20 mL of HCl solution, respectively. Then wet-algae was mixed with 250 mL of a 1.0 N Na_2CO_3 solution at pH 11.5 in a beaker and mechanically stirred for 2 h at 60 °C. Sodium alginate was removed from starting material and diluted with 800 mL of distilled water and then treated with 1 g of diatomaceous earth or activated charcoal. The resulting mixture was stirred for 15 min and the insoluble material removed by centrifugation, giving sodium ALG as product in the supernatant.

Appendix A.2 Purifying of ALG Extracted from L. nigrescens

A sodium ALG solution with 1M HCl (250 mL) was mixed until reaching a pH value of 2, and then kept at room temperature under stirring for 1 h. Further, the precipitated alginic acid was removed by centrifugation, and distilled water (100 mL) and 1.0 M Na_2CO_3 (150 mL) were added. The total mixture was left under stirring at room temperature for 1 h until soluble sodium ALG was obtained. After that, ALG was precipitated from this solution by slow addition of ethanol (volume 1/1). The resultant precipitate was purified by washing with ethanol through soxhlet extractor for 100 h, and dried under vacuum at room temperature, until reaching a constant mass [25,48].

References

1. Mann, S. *Biomineralization: Principles and Concepts in Bioinorganic Materials Chemistry*, 1st ed.; Oxford University Press: New York, NY, USA, 2001; pp. 1–30. ISBN 0198508824.
2. Arias, J.L.; Neira-Carrillo, A.; Arias, J.I.; Escobar, C.; Bodero, M.; David, M.; Fernández, M.S. Sulfated polymers in biological mineralization: A plausible source for bio-inspired engineering. *J. Mater. Chem.* **2004**, *14*, 2154–2160. [CrossRef]
3. Arias, J.L.; Fernández, M.S. Polysaccharides and proteoglycans in calcium carbonate-based biomineralization. *Chem. Rev.* **2008**, *108*, 4475–4482. [CrossRef] [PubMed]

4. Young, J.R.; Henriksen, K. Biomineralization within vesicles: The calcite of coccoliths. *Rev. Mineral. Geochem.* **2003**, *54*, 189–215. [CrossRef]
5. Boyjoo, Y.; Pareek, V.K.; Liu, J. Synthesis of micro and nano-sized calcium carbonate particles and their applications. *J. Mater. Chem. A* **2014**, *2*, 14270–14288. [CrossRef]
6. Gebauer, D.; Völkel, A.; Cölfen, H. Stable prenucleation calcium carbonate clusters. *Science* **2008**, *322*, 1819–1822. [CrossRef] [PubMed]
7. Gebauer, D.; Cölfen, H. Prenucleation clusters and non-classical nucleation. *Nano Today* **2011**, *6*, 564–584. [CrossRef]
8. Gebauer, D.; Kellermeier, M.; Gale, J.D.; Bergström, L.; Cölfen, H. Pre-nucleation clusters as solute precursors in crystallisation. *Chem. Soc. Rev.* **2014**, *43*, 2348–2371. [CrossRef] [PubMed]
9. Kellermeier, M.; Cölfen, H.; Gebauer, D. Investigating the early stages of mineral precipitation by potentiometric titration and analytical ultracentrifugation. *Methods Enzymol.* **2013**, *532*, 45–69. [PubMed]
10. Cartwright, J.H.; Checa, A.G.; Gale, J.D.; Gebauer, D.; Sainz-Díaz, C.I. Calcium carbonate polyamorphism and its role in biomineralization: How many amorphous calcium carbonates are there? *Angew. Chem. Int. Ed.* **2012**, *51*, 11960–11970. [CrossRef] [PubMed]
11. Chen, S.-F.; Cölfen, H.; Antonietti, M.; Yu, S.-H. Ethanol assisted synthesis of pure and stable amorphous calcium carbonate nanoparticles. *ChemComm* **2013**, *49*, 9564–9566. [CrossRef] [PubMed]
12. Rao, A.; Berg, J.K.; Kellermeier, M.; Gebauer, D. Sweet on biomineralization: Effects of carbohydrates on the early stages of calcium carbonate crystallization. *Eur. J. Miner.* **2014**, *26*, 537–552. [CrossRef]
13. Rao, A.; Vásquez-Quitral, P.; Fernández, M.S.; Berg, J.K.; Sánchez, M.; Drechsler, M.; Neira-Carrillo, A.; Arias J., L.; Gebauer, D.; Cölfen, H. pH-dependent schemes of calcium carbonate formation in the presence of alginates. *Cryst. Growth Des.* **2016**, *16*, 1349–1359. [CrossRef]
14. Neira-Carrillo, A.; Krishna Pai, R.; Fernández, M.S.; Carreño, E.; Vásquez-Quitral, P.; Arias, J.L. Synthesis and characterization of sulfonated polymethylsiloxane polymer as template for crystal growth of $CaCO_3$. *Colloid Polym. Sci.* **2009**, *287*, 385–393. [CrossRef]
15. Neira-Carrillo, A.; Vásquez-Quitral, P.; Díaz, M.P.; Fernández, M.S.; Arias, J.L.; Yazdani-Pedram, M. Control of calcium carbonate crystallization by using anionic polymethylsiloxanes as templates. *J. Solid State Chem.* **2012**, *194*, 400–408. [CrossRef]
16. Neira-Carrillo, A.; Vásquez Quitral, P.; Yazdani-Pedram, M.; Arias, J.L. Crystal growth of $CaCO_3$ induced by new carboxylated monomethylitaconate grafted polymethylsiloxane. *Eur. Polym. J.* **2010**, *46*, 1184–1193. [CrossRef]
17. Lee, K.Y.; Mooney, D.J. Alginate: Properties and biomedical applications. *Prog. Polym. Sci.* **2012**, *37*, 106–126. [CrossRef] [PubMed]
18. Asenath-Smith, E.; Li, H.; Keene, E.C.; Seh, Z.W.; Estroff, L.A. Crystal growth of calcium carbonate in hydrogels as a model of biomineralization. *Adv. Funct. Mater.* **2012**, *22*, 2891–2914. [CrossRef]
19. Salgado, L.T.; Amado Filho, G.M.; Fernández, M.S.; Arias, J.L.; Farina, M. The effect of alginates, fucans and phenolic substances from the brown seaweed *Padina gymnospora* in calcium carbonate mineralization in vitro. *J. Cryst. Growth* **2011**, *321*, 65–71. [CrossRef]
20. Manoli, F.; Dalas, E. The effect of sodium alginate on the crystal growth of calcium carbonate. *J. Mater. Sci. Mater. Med.* **2002**, *13*, 155–158. [CrossRef] [PubMed]
21. Olderøy, M.Ø.; Xie, M.; Strand, B.L.; Flaten, E.M.; Sikorski, P.; Andreassen, J.P. Growth and nucleation of calcium carbonate vaterite crystals in presence of alginate. *Cryst. Growth Des.* **2009**, *9*, 5176–5183. [CrossRef]
22. Ma, Y.; Feng, Q. Alginate hydrogel-mediated crystallization of calcium carbonate. *J. Solid State Chem.* **2011**, *184*, 1008–1015. [CrossRef]
23. Egaña Palma, R. Preparación de Esferas de Alginato Purificado de Origen Comercial y Desde Algas Chilenas *Lessonia nigrescens* Como Implante Para Terapia Celular. MVD Thesis, Facultad de Ciencias Veterinarias y Pecuarias, Universidad de Chile, Santiago, Chile, 2013.
24. Gebauer, D.; Cölfen, H.; Verch, A.; Antonietti, M. The multiple roles of additives in $CaCO_3$ crystallization: A quantitative case study. *Adv. Mater.* **2009**, *21*, 435–439. [CrossRef]
25. Xu, J.Z.; Zhong, G.J.; Hsiao, B.S.; Fu, Q.; Li, Z.M. Low-dimensional carbonaceous nanofiller induced polymer crystallization. *Prog. Polym. Sci.* **2014**, *39*, 555–593. [CrossRef]

26. Tasis, D.; Tagmatarchis, N.; Bianco, A.; Prato, M. Chemistry of carbon nanotubes. *Chem. Rev.* **2006**, *106*, 1105–1136. [CrossRef] [PubMed]
27. Makar, J.M.; Chan, G.W. Growth of cement hydration products on single-walled carbon nanotubes. *J. Am. Ceram. Soc.* **2009**, *92*, 1303–1310. [CrossRef]
28. Balázsi, C.; Wéber, F.; Kövér, Z.; Shen, Z.; Konya, Z.; Kasztovszky, Z.; Vértesy, Z.; Biró, L.P.; Kiricsi, I.; Arato, P. Application of carbon nanotubes to silicon nitride matrix reinforcements. *Curr. Appl. Phys.* **2006**, *6*, 124–130. [CrossRef]
29. Lupo, F.; Kamalakaran, R.; Scheu, C.; Grobert, N.; Rühle, M. Microstructural investigations on zirconium oxide–carbon nanotube composites synthesized by hydrothermal crystallization. *Carbon* **2004**, *42*, 1995–1999. [CrossRef]
30. Tasis, D.; Pispas, S.; Galiotis, C.; Bouropoulos, N. Growth of calcium carbonate on non-covalently modified carbon nanotubes. *Mater. Lett.* **2007**, *61*, 5044–5046. [CrossRef]
31. Li, W.; Gao, C. Efficiently stabilized spherical vaterite $CaCO_3$ crystals by carbon nanotubes in biomimetic mineralization. *Langmuir* **2007**, *23*, 4575–4582. [CrossRef] [PubMed]
32. Pavez, J.; Silva, J.F.; Melo, F. Effects of alginic acid from marine algae on calcium carbonate electrodeposited coating. *J. Cryst. Growth* **2005**, *282*, 438–447. [CrossRef]
33. Neira-Carrillo, A.; Acevedo, D.F.; Miras, M.C.; Barbero, C.A.; Gebauer, D.; Cölfen, H.; Arias, J.L. Influence of Conducting Polymers Based on Carboxylated Polyaniline on in vitro $CaCO_3$ Crystallization. *Langmuir* **2008**, *24*, 12496–12507. [CrossRef] [PubMed]
34. Neira-Carrillo, A.; Yazdani-Pedram, M.; Retuert, J.; Díaz-Dosque, M.; Gallois, S.; Arias, J.L. Selective crystallization of calcium salts by poly(acrylate)-grafted chitosan. *J. Colloid Interface Sci* **2005**, *286*, 134–141. [CrossRef] [PubMed]
35. Neira-Carrillo, A.; Retuert, J.; Martinez, F.; Arias, J.L. Effect of crosslinked chitosan as a constrained volume on the in vitro calcium carbonate crystallization. *J. Chil. Chem. Soc.* **2008**, *53*, 1367–1372. [CrossRef]
36. Neira-Carrillo, A.; Pai, R.; Fuenzalida, V.; Fernandez, M.S.; Retuert, J.; Arias, J.L. Calcium carbonate growth modification by constituents releases from porous cellulose filter membranes. *J. Chil. Chem. Soc.* **2008**, *53*, 1469–1473. [CrossRef]
37. Yang, X.; Kim, E.; Liu, Y.; Shi, X.W.; Rubloff, G.W.; Ghodssi, R.; Payne, G.F. In-film bioprocessing and immunoanalysis with electroaddressable stimuli-responsive polysaccharides. *Adv. Funct. Mater.* **2010**, *20*, 1645–1652. [CrossRef]
38. Lédion, J.; Leroy, P.; Labbé, J.-P. Détermination du caractère incrustant d'une eau par un essai d'entartrage accéléré. *Tech. Sci. Munic. (1971)* **1985**, *7–8*, 323–328.
39. Butler, M.F.; Glaser, N.; Weaver, A.C.; Kirkland, M.; Heppenstall-Butler, M. Calcium carbonate crystallization in the presence of biopolymers. *Cryst. Growth Des.* **2006**, *6*, 781–794. [CrossRef]
40. Díaz-Dosque, M.; Aranda, P.; Darder, M.; Retuert, J.; Yazdani-Pedram, M.; Arias, J.L.; Ruiz-Hitzky, E. Use of biopolymers as oriented supports for the stabilization of different polymorphs of biomineralized calcium carbonate with complex shape. *J. Cryst. Growth* **2008**, *310*, 5331–5340. [CrossRef]
41. Ketrane, R.; Saidani, B.; Gil, O.; Leleyter, L.; Baraud, F. Efficiency of five scale inhibitors on calcium carbonate precipitation from hard water: Effect of temperature and concentration. *Desalination* **2009**, *249*, 1397–1404. [CrossRef]
42. Butler, M.F.; Frith, W.J.; Rawlins, C.; Weaver, A.C.; Heppenstall-Butler, M. Hollow calcium carbonate microsphere formation in the presence of biopolymers and additives. *Cryst. Growth Des.* **2008**, *9*, 534–545. [CrossRef]
43. Qi, Y.; Jiang, M.; Cui, Y.L.; Zhao, L.; Zhou, X. Synthesis of quercetin loaded nanoparticles based on alginate for Pb (II) adsorption in aqueous solution. *Nanoscale Res. Lett.* **2015**, *10*, 408. [CrossRef] [PubMed]
44. Lakouraj, M.M.; Mojerlou, F.; Zare, E.N. Nanogel and superparamagnetic nanocomposite based on sodium alginate for sorption of heavy metal ions. *Carbohydr. Polym.* **2014**, *106*, 34–41. [CrossRef] [PubMed]
45. Leng, B.; Jiang, F.; Lu, K.; Ming, W.; Shao, Z. Growth of calcium carbonate mediated by slowly released alginate. *CrystEngComm* **2010**, *12*, 730–736. [CrossRef]
46. Neira-Carrillo, A.; Vásquez-Quitral, P.; Sánchez, M.; Farhadi-Khouzani, M.; Aguilar-Bolados, H.; Yazdani-Pedram, M.; Cölfen, H. Evaluation of functionalized multi-walled CNTs as template for classical and non-classical $CaCO_3$ crystallization. Unpublished work. 2018.

47. Zhao, B.; Hu, H.; Mandal, S.K.; Haddon, R.C. A Bone mimic based on the self-assembly of hydroxyapatite on chemically functionalized single-walled carbon nanotubes. *Chem. Mater.* **2005**, *17*, 3235–3241. [CrossRef]
48. Gomez, C.G.; Lambrecht, M.V.P.; Lozano, J.E.; Rinaudo, M.; Villar, M.A. Influence of the extraction–purification conditions on final properties of alginates obtained from brown algae (*Macrocystis pyrifera*). *Int. J. Biol. Macromol.* **2009**, *44*, 365–371. [CrossRef] [PubMed]